Supporting information

Ultra-low lattice thermal conductivity and enhanced mechanical properties of Cu and Sb co-doped SnTe thermoelectric material with a complex microstructure evolution

Samuel Kimani Kihoi,[1] U. Sandhya Shenoy,[2] Joseph Ngugi Kahiu,[3] Hyunji Kim,[1] D. Krishna Bhat,[4] and Ho Seong Lee[1],*

[1]School of Materials Science and Engineering, Kyungpook National University, 80 Daehak-ro, Buk-gu, Daegu, 41566, Republic of Korea

[2]Department of Chemistry, College of Engineering and Technology, Srinivas University, Mukka -574146, Mangalore, Karnataka, India

[3]Department of Hydrogen and Renewable Energy, Kyungpook National University, 80 Daehak-ro, Buk-gu, Daegu, 41566, Republic of Korea

[4]Department of Chemistry, National Institute of Technology Karnataka, Surathkal, Srinivasnagar -575025, Mangalore, Karnataka, India

*Corresponding author: hs.lee@knu.ac.kr

Number of pages: 10

Number of figures: 8

Number of tables: 2

EXPERIMENTAL SECTION

Synthesis. Highly pure Sn shot (99.999%), Te broken ingot (99.99%), Cu powder (99.9%) and Sb shot (99.9999%) metals basis from Alfa Aesar were weighed according to the stoichiometric ratio $Sn_{0.88-y}Cu_{0.12}Sb_yTe$ (y=0-0.15) and loaded in quartz ampoules. The ampoules were necked over a gas flame, vacuumed to 10^{-3} torr, purged with Ar gas, and sealed. Melting was then done in a rocking furnace at 950 °C for 12 h followed by homogenization in a box furnace for 48 h at 600 °C. The ingots were then hand ground to < 45 μm and densified in a DC hot press at 500 °C for 1 h with an axial load of 80 MPa. The resulting cylindrical billets were then cut accordingly for various characterization processes.

Material characterization. X-ray diffraction was done using a Rigaku D/Max-2500 X-ray diffractometer for $2\theta = 20 - 80^o$ in steps of 0.02^o. A Cu Kα (λ=1.5406 Å) radiation was used. Microstructure analysis was done by both Hitachi SU8220 Field Emission Scanning Electron Microscope (FE-SEM) and Titan G2 ChemiSTEM Cs probe Field Emission Transmission Electron Microscope (FE-TEM) operating at 200 kV, both with an Energy Dispersive X-ray Spectroscopy (EDS) detector. Thermogravimetric Analysis and Differential Scanning Calorimetry (TGA-DSC) measurements were done using a TA Instruments (Discovery SDT 650) Auto TGA-DSC for the temperature range room temperature – 600 °C in a N_2 atmosphere. Electronic properties Seebeck coefficient (*S*) and electrical conductivity (*σ*) were simultaneously measured in a He atmosphere using a BluSys 1 (BS1) machine. Room temperature Hall measurements were done using the Van der Pauw method in an Ecopia four-point probe Hall Effect Measurement System. Thermal diffusivity (*D*) (Fig. S6) was measured using the Laser Flash Analysis method in an ULVAC TC-9000H instrument. Density (*ρ*) of all samples was done using the Archimedes' method. The specific heat capacity (*C_p*) was calculated using the Dulong-Petit law. Then, the total thermal conductivity was determined through $\kappa = DC_p\rho$. The electron contribution to heat transfer was calculated as, $\kappa_e = L\sigma T$,

where L is the Lorenz number (Fig. S7) calculated as $L = 1.5 + exp[-|S|/116]$ in 10^{-8} WΩK^{-2}. The phonon contribution was thus determined as, $\kappa_{lat} = \kappa - \kappa_e$. Microhardness of all samples was done using an emcoTEST Durascan 10 Vickers hardness tester.

Computation details. We used Quantum ESPRESSO package to study the electronic structure of pristine, doped, and co-doped SnTe.[1] Density functional theory (DFT) calculations, based on first principles were carried out using fully relativistic ultrasoft pseudopotentials of Perdew, Burke and Erzenhoff (PBE) functional type.[2] Spin orbit coupling interaction was considered during the simulations. A generalized gradient approximation was used in the determination of total energies. A ($\sqrt{2} \times \sqrt{2} \times 2$) a_o supercell with 32 atoms was used for the DFT calculations. The wavefunctions represented by plane wave basis were terminated with an energy cutoff of 50 Ry and charge density cutoff of 400 Ry. Self-consistent field calculations were performed with $14 \times 14 \times 10$ k mesh. Electronic structure was determined along X-M-Γ-Z-R-A path in the Brillouin zone.

Supporting figures
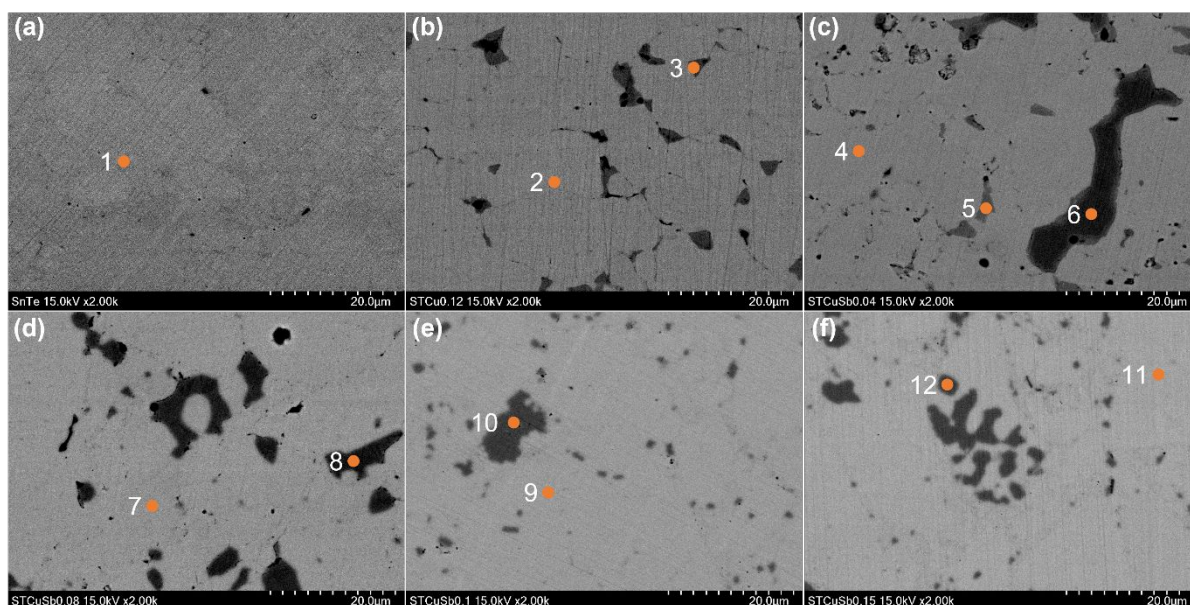
Fig. S1: FE-SEM BSE images for the (a) SnTe, (b) $Sn_{0.88}Cu_{0.12}Te$, (c) $Sn_{0.84}Cu_{0.12}Sb_{0.04}Te$, (d) $Sn_{0.80}Cu_{0.12}Sb_{0.08}Te$, (e) $Sn_{0.78}Cu_{0.12}Sb_{0.10}Te$, and (f) $Sn_{0.73}Cu_{0.12}Sb_{0.15}Te$ compositions.

Table S1. EDS point mapping for the FESEM BSE images in Fig. S1

Composition	Point	Atomic %			
		Sn	**Cu**	**Sb**	**Te**
SnTe	1	52.24	0.00	0.00	47.76
$Sn_{0.88}Cu_{0.12}Te$	2	50.13	2.54	0.00	47.05
	3	15.20	37.94	0.00	46.86
$Sn_{0.84}Cu_{0.12}Sb_{0.04}Te$	4	47.35	2.66	2.48	47.51
	5	17.12	38.00	0.18	44.69
	6	1.20	59.22	0.27	39.31
$Sn_{0.80}Cu_{0.12}Sb_{0.08}Te$	7	44.71	1.92	4.94	48.44
	8	0.22	64.25	0.00	35.53
$Sn_{0.78}Cu_{0.12}Sb_{0.10}Te$	9	43.57	1.86	5.75	48.82
	10	0.30	65.17	0.03	34.50
$Sn_{0.73}Cu_{0.12}Sb_{0.15}Te$	11	40.47	3.54	7.97	48.02
	12	0.46	66.29	0.06	33.19
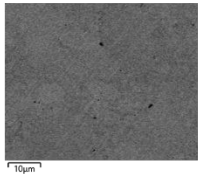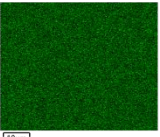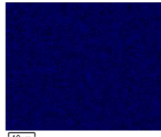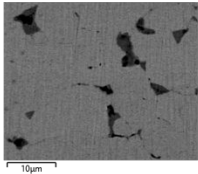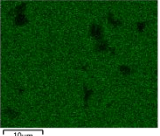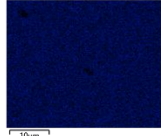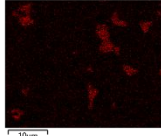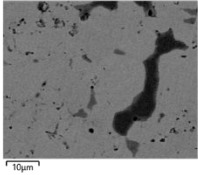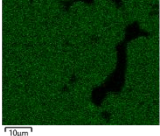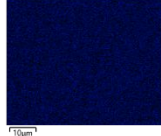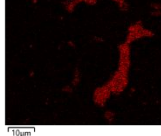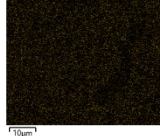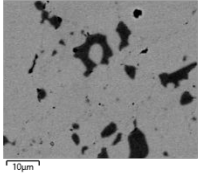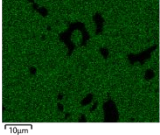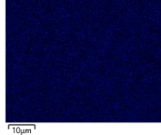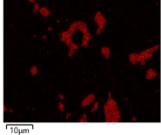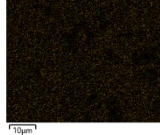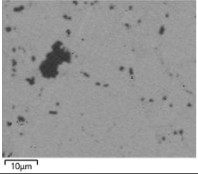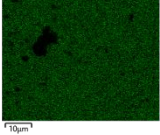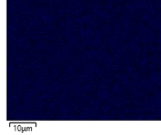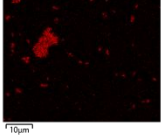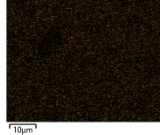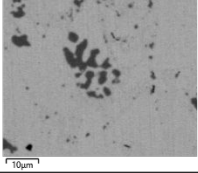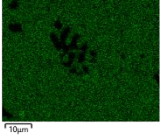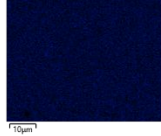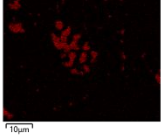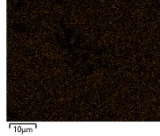
Composition		Sn	Te	Cu	Sb
(a) SnTe					
(b) $Sn_{0.88}Cu_{0.12}Te$					
(c) $Sn_{0.84}Cu_{0.12}Sb_{0.04}Te$					
(d) $Sn_{0.80}Cu_{0.12}Sb_{0.08}Te$					
(e) $Sn_{0.78}Cu_{0.12}Sb_{0.10}Te$					
(f) $Sn_{0.73}Cu_{0.12}Sb_{0.15}Te$					

Fig. S2. FE-SEM EDS mapping for various $Sn_{0.88-y}Cu_{0.12}Sb_yTe$ compositions in Fig. S1.
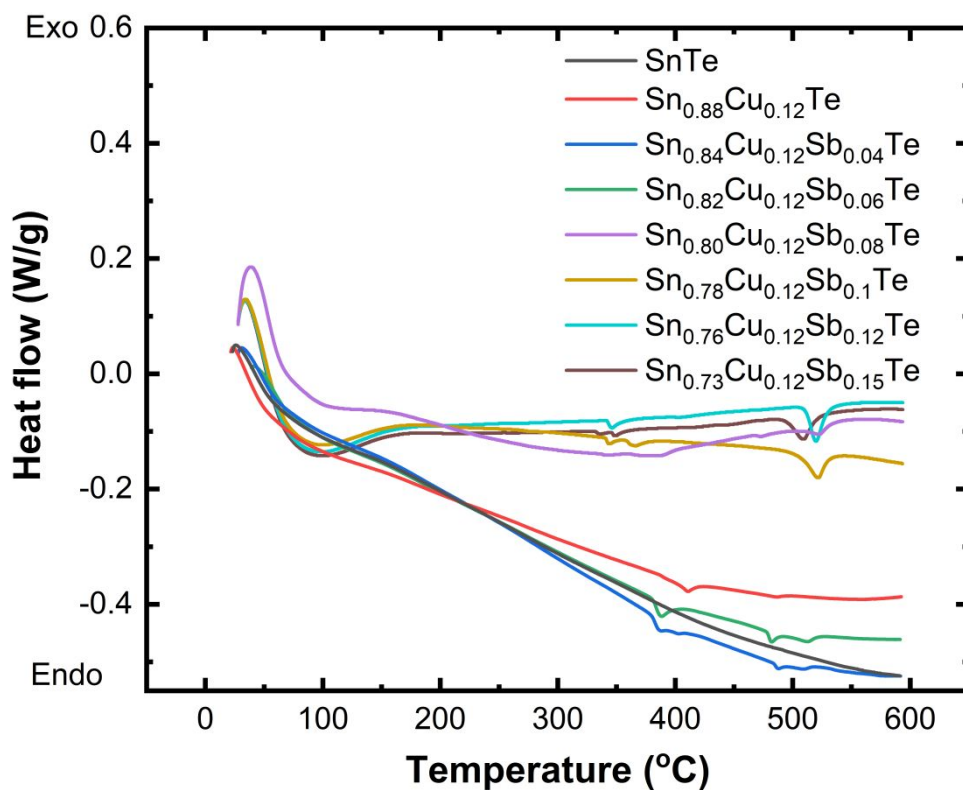
Fig. S3. DSC profiles for the $Sn_{0.88-y}Cu_{0.12}Sb_yTe$ compositions.

Table S2. Summary of the peak melting temperature, T_m for the $Sn_{0.88-y}Cu_{0.12}Sb_yTe$ compositions

Composition	Various peak melting temperatures (ºC)			
	T_1	T_2	T_3	T_4
SnTe				
$Sn_{0.88}Cu_{0.12}Te$		410.51	486.33	
$Sn_{0.84}Cu_{0.12}Sb_{0.04}Te$		386.77	487.80	
$Sn_{0.82}Cu_{0.12}Sb_{0.06}Te$		387.93	482.01	
$Sn_{0.80}Cu_{0.12}Sb_{0.08}Te$	341.73	388.51		522.68
$Sn_{0.78}Cu_{0.12}Sb_{0.10}Te$	343.62			521.62
$Sn_{0.76}Cu_{0.12}Sb_{0.12}Te$	346.38			519.94
$Sn_{0.73}Cu_{0.12}Sb_{0.15}Te$	348.87			509.52
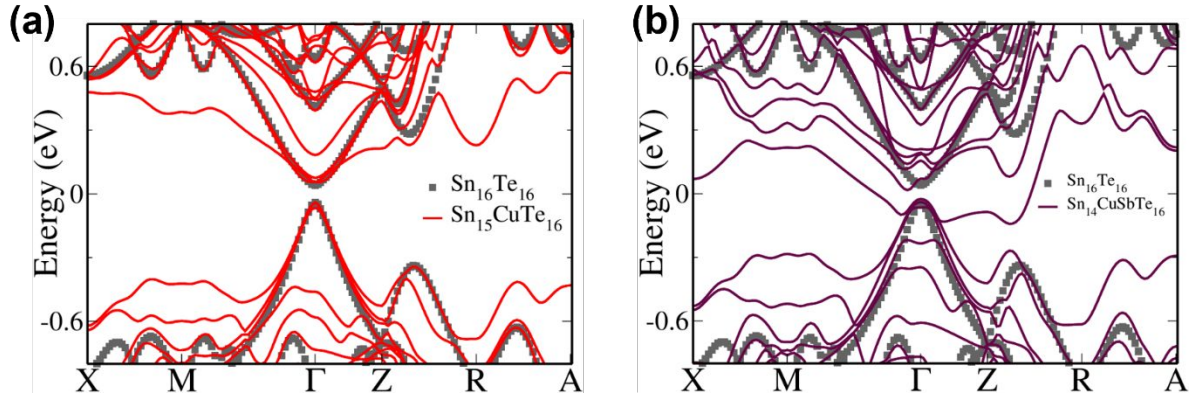
Fig. S4. Comparison of the electronic structure between SnTe and (a) Cu and (b) Cu-Sb co-doped SnTe, respectively.
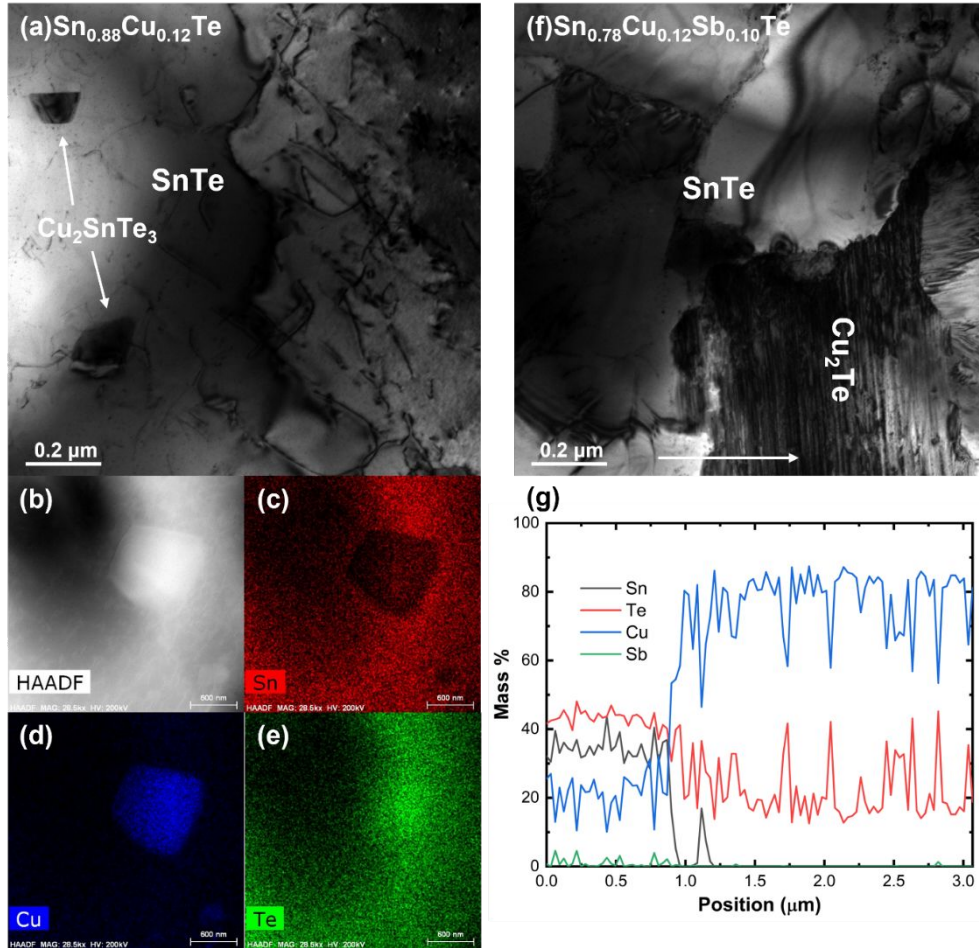
Fig. S5. FE-TEM bright field (BF) images for (a)$Sn_{0.88}Cu_{0.12}Te$ and (b-e) EDS mapping for a sample second phase within the matrix and (f) $Sn_{0.78}Cu_{0.12}Sb_{0.10}Te$ and (g) corresponding line scan along the white arrow.
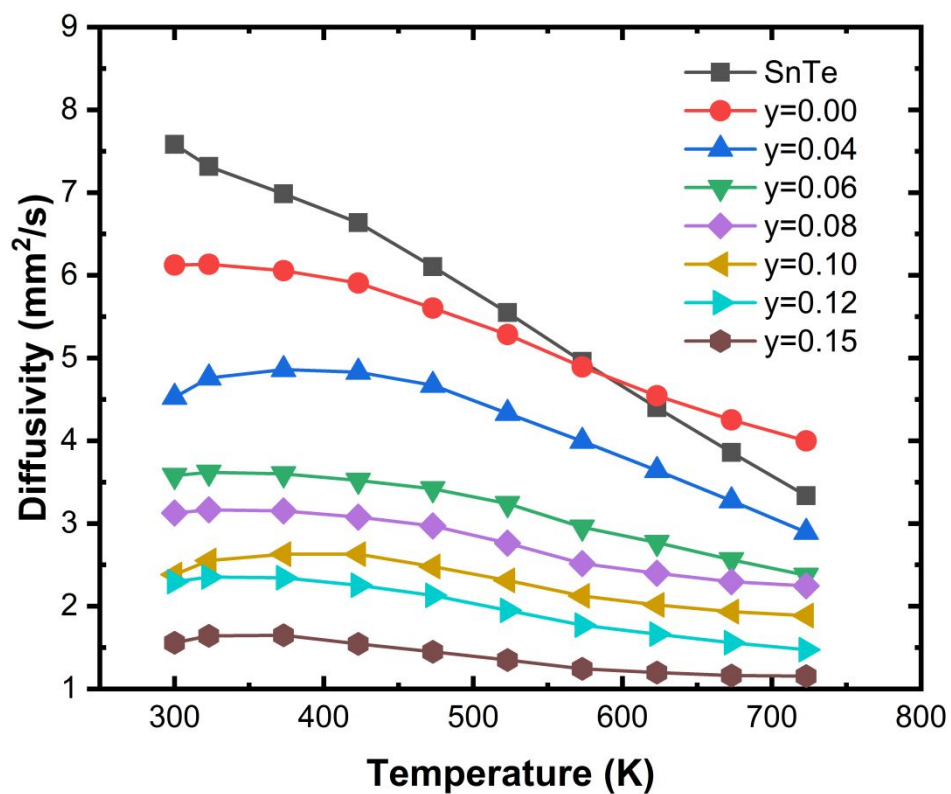
Fig. S6. Temperature dependent diffusivity for the $Sn_{0.88-y}Cu_{0.12}Sb_yTe$ compositions.
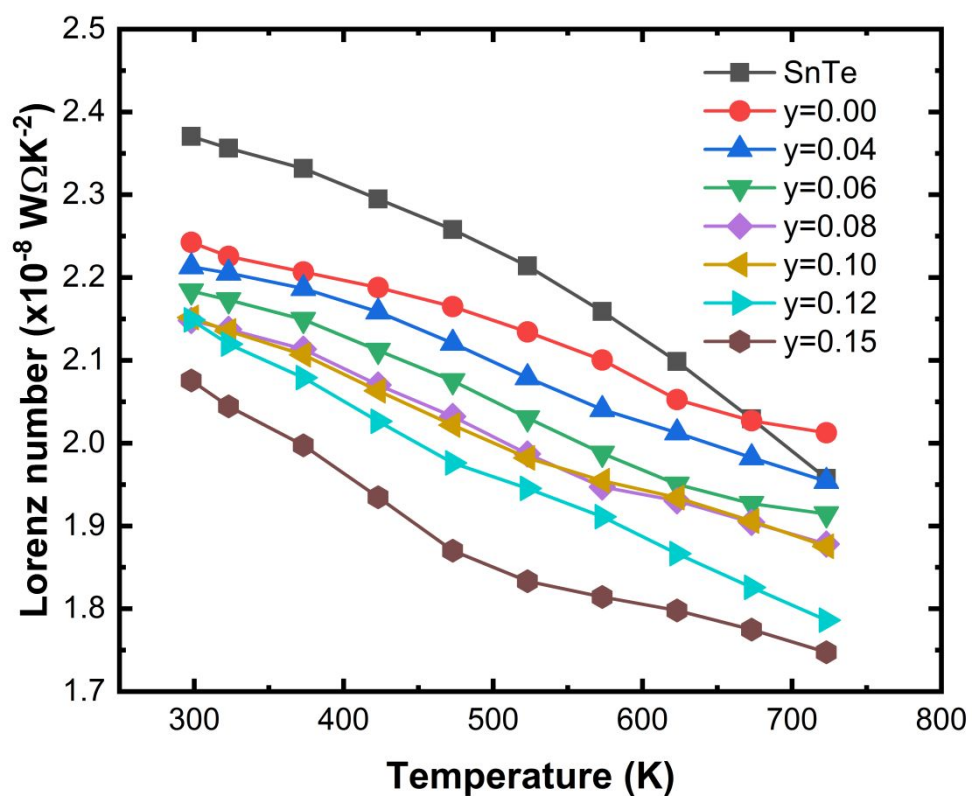
Fig. S7. Temperature dependent Lorenz number for the $Sn_{0.88-y}Cu_{0.12}Sb_yTe$ compositions.

Fig. S8. Comparison of various hardness (Hv) values for various SnTe doped samples including

Ge,[3] PbTe@C,[4] SiC,[5] MnBiSb,[6] Sb (melt spinning),[7] ZnSb,[8] BiSb,[9] Sb[10] and hot deformed (HD)

SnTe[11] with this work's CuSb co-doped sample.

REFERENCES

(1)   Giannozzi, P.; Baroni, S.; Bonini, N.; Calandra, M.; Car, R.; Cavazzoni, C.; Ceresoli, D.; Chiarotti, G. L.; Cococcioni, M.; Dabo, I.; Dal Corso, A.; De Gironcoli, S.; Fabris, S.; Fratesi, G.; Gebauer, R.; Gerstm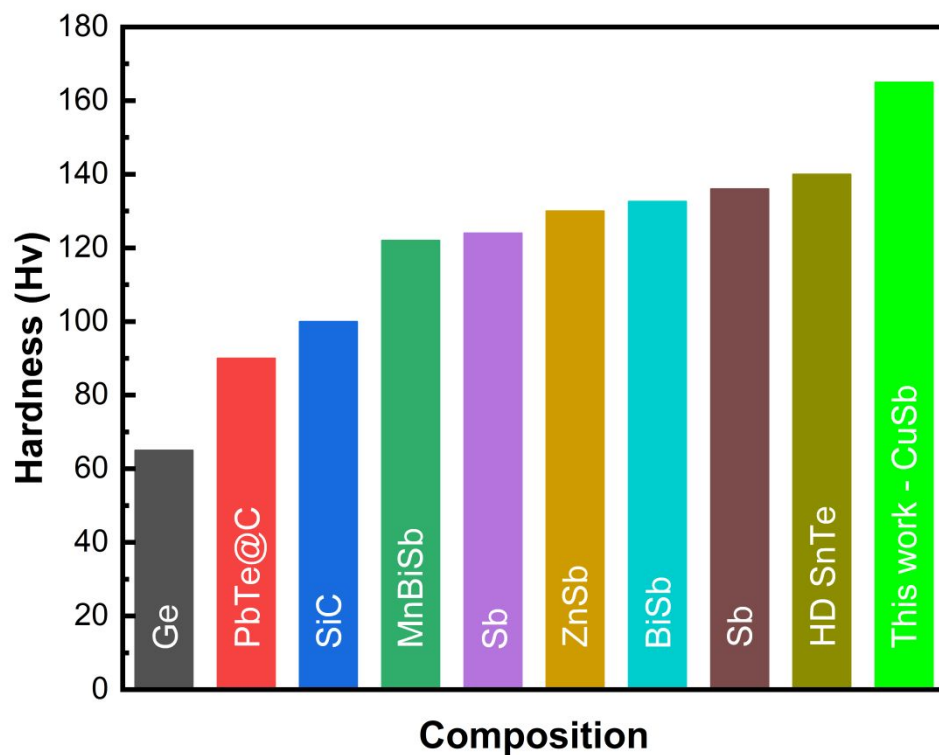ann, U.; Gougoussis, C.; Kokalj, A.; Lazzeri, M.; Martin-Samos, L.; Marzari, N.; Mauri, F.; Mazzarello, R.; Paolini, S.; Pasquarello, A.; Paulatto, L.; Sbraccia, C.; Scandolo, S.; Sclauzero, G.; Seitsonen, A. P.; Smogunov, A.; Umari, P.; Wentzcovitch, R. M. QUANTUM ESPRESSO: A Modular and Open-Source Software Project for Quantum Simulations of Materials. *J. Phys. Condens. Matter* **2009**, *21* (39), 395502. https://doi.org/10.1088/0953-8984/21/39/395502.

(2)   Perdew, J. P.; Burke, K.; Ernzerhof, M. Generalized Gradient Approximation Made Simple. *Phys. Rev. Lett.* **1996**, *77* (18), 3865–3868. https://doi.org/10.1103/PhysRevLett.77.3865.

(3)   Aminzare, M.; Tseng, Y. C.; Ramakrishnan, A.; Chen, K. H.; Mozharivskyj, Y. Effect of Single Metal Doping on the Thermoelectric Properties of SnTe. *Sustain. Energy Fuels* **2019**, *3* (1), 251–263. https://doi.org/10.1039/c8se00385h.

(4)   Zhang, J.; Li, S.; Zhu, Z.; Wu, Z.; Zhang, J. Enhancing the Thermoelectric Properties of SnTe via Introducing PbTe@C Core-Shell Nanostructures. *Dalt. Trans.* **2021**, *50* (30), 10515–10523. https://doi.org/10.1039/d1dt01725j.

(5)   Wang, T.; Wang, H.; Su, W.; Zhai, J.; Yakovleva, G.; Wang, X.; Chen, T.; Romanenko, A.; Wang, C. Simultaneous Enhancement of Thermoelectric and Mechanical Performance for SnTe by Nano SiC Compositing. *J. Mater. Chem. C* **2020**, *8* (22), 7393–7400. https://doi.org/10.1039/d0tc00572j.

(6)   Kihoi, S. K.; Kim, H.; Jeong, H.; Kim, H.; Ryu, J.; Yi, S.; Lee, H. S. Thermoelectric Properties of Mn, Bi, and Sb Co-Doped SnTe with a Low Lattice Thermal Conductivity. *J. Alloys Compd.* **2019**, *806*, 361–369. https://doi.org/10.1016/j.jallcom.2019.07.220.

(7)   Yang, B.; Li, S.; Li, X.; Liu, Z.; Zhong, H.; Feng, S. Ultralow Thermal Conductivity and Enhanced Thermoelectric Properties of SnTe Based Alloys Prepared by Melt Spinning Technique. *J. Alloys Compd.* **2020**, *837*, 155568. https://doi.org/10.1016/j.jallcom.2020.155568.

(8)   Kihoi, S. K.; Lee, H. S. Nanostructuring SnTe to Improve Thermoelectric Properties through Zn and Sb Co-Doping. *Sustain. Energy Fuels* **2020**, *4* (11), 5645–5653. https://doi.org/10.1039/d0se01081b.

(9)   Kihoi, S. K.; Shenoy, U. S.; Bhat, D. K.; Lee, H. S. Complementary Effect of Co-Doping Aliovalent Elements Bi and Sb in Self-Compensated SnTe-Based Thermoelectric Materials. *J. Mater. Chem. C* **2021**, *9* (31), 9922–9931. https://doi.org/10.1039/d1tc01676h.

(10)   Banik, A.; Vishal, B.; Perumal, S.; Datta, R.; Biswas, K. The Origin of Low Thermal Conductivity in $Sn_{1-x}Sb_xTe$: Phonon Scattering via Layered Intergrowth Nanostructures. *Energy Environ. Sci.* **2016**, *9* (6), 2011–2019. https://doi.org/10.1039/c6ee00728g.

(11)   Li, S.; Xin, J.; Li, W.; Tao, Y.; Xu, T.; Xiao, B.; Luo, Y.; Jiang, Q.; Yang, J. Enhanced Thermoelectric Performance of Orientated and Defected SnTe. *J. Alloys Compd.* **2021**, *858*, 157634. https://doi.org/10.1016/j.jallcom.2020.157634.